Journal of Molecular Catalysis A: Chemical 349 (2011) 1–12

Contents lists available at SciVerse ScienceDirect

Journal of Molecular Catalysis A: Chemical

journal homepage: www.elsevier.com/locate/molcata

Editor's choice paper

Activity of chromium oxide deposited on different silica supports in the dehydrogenation of propane with CO_2 – A comparative study

Piotr Michorczyk*, Jan Ogonowski, Kamila Zeńczak

Institute of Organic Chemistry and Technology, Cracow University of Technology, ul. Warszawska 24, PL 31-155 Kraków, Poland

ARTICLE INFO

Article history:
Received 10 May 2011
Received in revised form 16 August 2011
Accepted 20 August 2011
Available online 27 August 2011

Keywords:
Chromium oxide catalysts
Redox Cr species
Silica supports
Dehydrogenation with CO_2
Propene

ABSTRACT

Four series of chromium oxide-based catalysts containing 0.7–7 wt.% of Cr were prepared by incipient wetness impregnation of conventional amorphous silicas (SiO_2-p; S_{BET} = 261 $m^2\ g^{-1}$ and SiO_2-a; S_{BET} = 477 $m^2\ g^{-1}$) and mesoporous siliceous sieves with cubic (SBA-1; S_{BET} = 1181 $m^2\ g^{-1}$) and hexagonal (SBA-15; S_{BET} = 750 $m^2\ g^{-1}$) pore structure. The combination of different techniques (chemical analysis with Bunsen–Rupp method, ICP, XRD, UV–vis DRS and quantitative/qualitative H_2-TPR) in the characterization of the calcined catalysts revealed that the chromium species anchored on the surface of mesoporous supports show structural properties similar to those on the conventional silicas, but a higher dispersion of chromium species could be achieved using mesoporous supports due to their much higher S_{BET}. This reflects in higher content of Cr^{6+} species stabilized in comparison with conventional silicas. The Cr^{6+} species was found to be crucial for high activity in the dehydrogenation of propane with CO_2 (DHP–CO_2). The rate of propene formation increases almost proportionally to the concentration of Cr^{6+} species in the calcined catalysts. *In situ* UV–vis DRS measurements during DHP–CO_2 process evidences that the Cr^{6+} species are reduced rapidly (in a stream of CO_2 + propane) to Cr^{3+} and Cr^{2+} species indicating that the Cr^{6+} species are rather precursor than active sites, similar as in nonoxidative dehydrogenation of propane (DHP). The reduction of Cr^{6+} species generates dispersed Cr^{3+} and Cr^{2+} sites at the beginning of the DHP–CO_2 that participate in nonoxidative pathway of propene formation. In the presence of CO_2, Cr^{3+} and Cr^{2+} sites, may participate additionally in an alternative oxidative pathway of propene formation and in a consumption of hydrogen produced in the DHP by reverse water-gas shift reaction.

1. Introduction

Dehydrogenation of light alkanes in the presence of CO_2 is considered to be one of the alternative methods of obtaining valuable alkenes with a higher yield than in the non-oxidative dehydrogenation variation, as well as a method of chemical CO_2 utilization. Many recent investigations have focused on dehydrogenation of propane to propene in the presence of CO_2. These investigations have been encouraged by a strong demand for propene, which has become one of the most important petrochemicals used for the production of a variety of polymers and chemical intermediates, such as: polypropylene, acrylonitile, OXO alcohols, isopropyl alcohol, acrylic acid and propylene oxide.

So far, different bulk and supported oxide-based materials containing active species, such as: Cr [1–14], Ga [6,14–20], Zn [21], Fe [22], V [10,23,24], In [25,26] and Mn [27,28] have been investigated as catalysts for dehydrogenation of propane in the presence of CO_2.

The results of these investigations lead to the following general conclusions:

(i) In the presence of CO_2, propene is obtained simultaneously with dehydrogenation and oxidative dehydrogenation pathways. The promoting effect of CO_2 is explained either by its participation in direct oxidation of propane to propene (1) or the consumption of hydrogen in the reverse water-gas shift reaction – RWGS (2), which shifts the equilibrium of propane dehydrogenation (3).

$$C_3H_8 + CO_2 \leftrightarrows C_3H_6 + CO + H_2O \quad (1)$$

$$CO_2 + H_2 \leftrightarrows CO + H_2O \quad (2)$$

$$C_3H_8 \leftrightarrows C_3H_6 + H_2 \quad (3)$$

The first, direct oxidative pathway with CO_2 was proposed in the case of redox oxides (Cr, V and Fe), whereas in the case of nonredox materials, such as gallium oxide-based catalysts, CO_2 participates mainly in the removal of H_2 in the reverse water-gas shift reaction.

(ii) The oxide catalysts which are active in the non-oxidative dehydrogenation of propane are also active in the process with CO_2.

* Corresponding author. Tel.: +48 12 628 27 29; fax: +48 12 628 20 37.
E-mail address: pmichor@pk.edu.pl (P. Michorczyk).

1381-1169/$ – see front matter © 2011 Elsevier B.V. All rights reserved.
doi:10.1016/j.molcata.2011.08.019

Among the investigated materials, those containing Cr or Ga were found to be the most active and selective.

(iii) Depending on the nature of the support, CO_2 has a promoting or poisoning effect on its catalytic properties. This can be seen most clearly in the case of supported chromium and gallium oxide materials. CO_2 has a negative effect on the Cr_2O_3/Al_2O_3 catalyst, while a promoting effect is observed over the Cr_2O_3/SiO_2 catalyst [8,9,13]. In the case of gallium oxide materials, CO_2 enhances the dehydrogenation activity of the Ga_2O_3/TiO_2 catalyst but suppresses that of the Ga_2O_3/Al_2O_3 and Ga_2O_3/ZrO_2 catalysts [17].

The catalytic activity of silica-supported chromium oxide materials (Cr/silica) depends on several factors including oxidation states, the structure of the Cr species and chromium–silica interaction. These factors are influenced by the type of the Cr precursor, preparation conditions (e.g., calcination temperature), Cr content and the properties of the silica support (e.g. iso-electric point – IEP) [29–31]. Cr species on 3+, 5+ and 6+ oxidation states coexist on the surface of oxidized Cr/silica catalysts. Below the monolayer coverage of silica, Cr species in the higher oxidation states, mainly as Cr^{6+} species in the form of mono- and polychromates, dominate. These highly dispersed and fully accessible for reactants species are believed to be the active sites or the precursors of the active sites [2,4,32–35]. When the Cr content exceeds the monolayer coverage, amorphous and crystalline α-Cr_2O_3 are formed [35]. The formation of crystalline α-Cr_2O_3, which is the most thermodynamically stable chromium oxide phase, is accelerated by high temperature and by the excess of water [30]. The presence of α-Cr_2O_3 on the surface of silica has a negative influence on the catalytic activity as not all of the Cr atoms are accessible to the reactant molecules. Moreover, crystalline α-Cr_2O_3 is highly resistant to hydrogen and oxygen what makes it useless as a catalyst [30].

The above general description concerning Cr/SiO_2 systems indicates that for obtaining a high activity, a high dispersion of Cr species has to be achieved. Therefore, more attention has been recently paid to using high surface area mesoporous materials as the supports for dispersing of chromium species. These materials possess a 2–4 times larger surface area than the commercial silica gels and have a uniform pore structure. So far, different Cr-containing mesoporous sieves (MCM-41, SBA-1, SBA-15 and MSU-x) prepared with various techniques have been investigated in dehydrogenation of propane with CO_2 [1,3–5,7,11,12].

In this work we presented a comparative study of the catalytic performance of chromium oxide supported on different siliceous supports including mesoporous sieves with cubic (SBA-1) and hexagonal (SBA-15) pore structure and two commercially available silica. Using various physicochemical characterization techniques we investigated the influence of Cr loading and supports properties on the surface composition and Cr dispersion. Finally based on the characterization results of catalysts we discussed the catalytic performance in the DHP–CO_2 process.

2. Experimental

2.1. Preparation of mesoporous supports and catalysts

Cetyltriethylammonium bromide (CTEABr) was synthesized by reaction of 1-bromohexadecane (97%, Aldrich) with an equimolar amount of triethylamine (98%, Fluka) in ethanol (99.8%, Chempur) under reflux for 72 h. The surfactant cetyltriethylammonium bromide (CTEABr) was purified by recrystallization from chloroform/ethyl acetate mixture [36].

SBA-1 was prepared under acidic conditions using CTEABr as the surfactant and tetraethyl orthosilicate (TEOS) as the silica source according to a literature procedure [37]. In a typical synthesis, 10 g of CTEABr, 1157 cm^3 of distilled water and 566 cm^3 of hydrochloric acid (37%, Chempur) were combined to form a homogeneous solution, which was cooled to 0 °C and stirred (400 rpm) for 30 min. Then 27.90 cm^3 of TEOS (98%, Aldrich) precooled to 0 °C was added, while vigorous stirring. The molar composition of the reaction mixture was TEOS:CTEABr:HCl:H_2O = 1:0.2:56:700. Stirring was continued for 4 h until precipitation of the silica-surfactant assemblies was complete. Next, the material formed at 0 °C was aged in the reaction mixture by heating at 100 °C for 1 h, to improve cross-linking of the silica framework. The resultant precipitate was filtered off and dried (without washing) at 60 °C overnight. This material was washed with ethanol–water–HCl mixture, dried and then calcined in air by rising temperature from ambient to 550 °C over 9 h period and then keeping it at 550 °C for another 12 h.

SBA-15 was synthesized under acidic conditions using Pluronic P123 triblock copolymer ($EO_{20}PO_{70}EO_{20}$, M_{av} = 5800, from Aldrich) and tetraethyl orthosilicate (TEOS) as the silica source. In a polypropylene bottle, 8 g of Pluronic P123 was dissolved in a solution containing 60 g of distilled water and 120 g of 2 M HCl at 35 °C. The mixture was vigorously stirred until complete dissolution of Pluronic P123. Next, 17 g of TEOS (98%, Aldrich) was added dropwise to the clear solution, while continues stirring (400 rpm) at 35 °C. Finally, the mixture was stirred (400 rpm) for another 20 h at 35 °C and then hydrothermally treated under static conditions for 24 h at 90 °C. The resultant white precipitate was filtered off without washing, dried overnight at 60 °C and calcined as SBA-1 material.

Catalysts with 0.7, 2.1, 3.4 and 6.8 wt.% of Cr were prepared by the incipient wetness method using $Cr(NO_3)_3{\cdot}9H_2O$ (Polish Chemical Reagents, POCh) as a chromium source. Before the impregnation all of the silica supports were dried for 12 h at 120 °C. Typically, 1 g of a mesoporous support (SBA-1 or SBA-15) was treated with 4.0 cm^3 of an aqueous solution containing the desired amount of $Cr(NO_3)_3$, while 1 g of a commercial silica material (SiO_2-p from POCh or SiO_2-a from Aldrich) was treated with 0.8 cm^3 of the precursor solution. The impregnated samples were dried at room temperature overnight, then for 6 h at 60 °C and finally calcined at 550 °C for 6 h in air. According the above procedure, four series of catalysts were obtained and were designated as Cr*x*/SBA-1, Cr*x*/SBA-15, Cr*x*/SiO_2-a and Cr*x*/SiO_2-p, respectively, where *x* expresses the establish Cr content in wt.% of Cr.

2.2. Characterization

Total Cr content (Cr_{tot}) in the catalysts was determined by ICP spectrometry (Perkin Elmer ELAN 6100). The catalysts samples were dissolved in a mixture of HF and HNO_3.

The amount of Cr^{6+} species in the fresh catalysts was determined by chemical analysis (Bunsen–Rupp method) [38]. The method relies on treating a sample of fresh catalyst with concentrated HCl which leads to reduction of Cr^{6+} ions to Cr^{3+}, according to the formal reaction: $Cr_2O_7^{2-} + 6Cl^- + 14H^+ = 3Cl_2 + 2Cr^{3+} + 7H_2O$. The evolved Cl_2 is quantitatively determined by iodometric titration. It should be noted that in this method, Cr^{5+} species (if present in the sample) are determined together with Cr^{6+} species. However, the amount of the former species in the supported catalysts was assumed to be small, typically below a few percent of the total Cr content [39,40]. The apparatus for performing the analysis was described by Dereń et al. [41]. In a typical procedure, 200 mg of fresh catalysts was placed into a vessel and after purification in argon flow, 20 cm^3 of HCl (36 wt.%, POCh) was added. In order to accelerate evolving of Cl_2, the mixture was heated up to 80 °C for 0.5 h. During the heating, the mixture of gases (Ar, Cl_2, H_2O and HCl) was passed through a second vessel filled with 0.1 M solution of KI (100 cm^3). The iodine

evolved in the potassium iodide solution was titrated with 0.05 M $Na_2S_2O_3$ in the presence of starch.

Nitrogen adsorption–desorption isotherms were measured at −196 °C using a Quantachrome Autosorb-1 instrument. The samples were degassed at 250 °C before measurements. Specific surface area was calculated using the Brunauer–Emmett–Teller (BET) method within the relative pressure range $P/P_0 = 0.05–0.25$. Pore size distribution was determined from the branch of the adsorption curve, using the Barrett–Joyner–Halenda (BJH) model. Pore volume was obtained from the volumes of nitrogen adsorbed at $P/P_0 = 0.95$ or vicinity.

Powder X-ray diffraction (XRD) patterns of pure mesoporous materials and catalysts were collected on a Panalytical X'Pert Pro instrument, operated at 40 kV and 30 mA, equipped with a Cu Kα X-ray (λ = 0.154 nm) radiation. The diffractograms were recorded in two ranges of 2 Theta (0.5–6.5° and 5–70°) with a 2 Theta step size 0.0167°, at room temperature.

Scanning electron microscope (SEM) images were collected using JEOL JSM-7500F instrument. For SEM observation mesoporous silica materials were deposited on the sample holder "as received".

Diffuse reflectance UV–vis (UV–vis DR) spectra were taken on an Ocean Optics HR2000+ instrument (integration time 400 ms, 100 scans) equipped with an Ocean Optics DH-2000 BAL halogen–deuterium light source at room temperature. The spectra were recorded within the wavelength range of 210–800 nm using $BaSO_4$ as a standard. The spectra are shown in a Kubelka–Munk format ($F(R) = (1-R)^2/2R$; where R – reflectance).

Temperature-programmed reduction (TPR) experiments were carried out on a modified gas chromatograph, equipped with a thermal conductivity detector (TCD) and connected on-line with a quartz reactor. Purified mixture of N_2/H_2 (95/5 vol.%, Air Liquide) served as a combined carrier and reducing gas at a total flow rate 30 $cm^3\ min^{-1}$. The flow rate of the reduction mixture was regulated by mass flow controller. Before H_2-TPR experiments, all the samples were dried for 12 h at 120 °C. The dry catalyst sample (100 mg) was preheated in air (99.96 vol.%, Linde) at 550 °C for 30 min and then in dry He (99.999 vol.%, Linde,) stream for next 30 min. Finally, the sample was cooled down in the He stream and the H_2-TPR experiments were carried out. The temperature was raised from 100 to 650 °C at a ramp rate 10 °C min^{-1}. The H_2 consumption was measured by a thermal conductivity detector and NiO (99.999%, Aldrich) was used as a reference for the calibration of H_2 consumption.

2.3. Catalytic tests

The dehydrogenation of propane (99.6 vol.%, Linde) in the presence of CO_2 (99.996 vol.%, Linde) was carried out in a flow-type quartz reactor. The reactor was a single quartz piece with two sections: inlet section has 10 mm in internal diameter and 150 mm long and an outlet section has 6 mm internal diameter and 120 mm long. The two sections are tapered and the catalysts bed was located on quartz wool just above the tapered region. The rector was packed with 200 mg of the catalyst (grain size 0.2–0.3 mm). The catalyst was preheated in a stream of dry argon (99.999 vol.%, Linde) for 30 min at 550 °C before each test, and then the reaction was started at set temperature (550 or 650 °C) under atmospheric pressure. The dehydrogenation feed consisted of a mixture of CO_2:C_3H_8:He = 5:1:9. The total flow rate was 30 $cm^3\ min^{-1}$. Test on the empty reactor indicates that at 650 °C propane conversion not exceeds 2.5%. Calculation based on published criteria [42] indicates that no heat and mass transfer limitation exists under reaction conditions applied in this paper.

The reactants and products were analyzed on-line using a gas chromatograph (Agilent 6890N) equipped with two columns (Hayesep Q and molecular sieve 5A) and a thermal conductivity detector. The column packed with Hayesep Q was used for separation of H_2, CO_2, C_2H_4, C_2H_6, C_3H_6 and C_3H_8. The molecular sieve 5A was used for the separation of CH_4 and CO.

Reaction rate normalized per catalyst weight (activity), conversion of propane, yield of propene and selectivity to all hydrocarbon products were calculated as described below.

$$\text{activity}(\text{mol}_{C_8H_8}\ s^{-1}\ g^{-1}) = F_p \times C_p$$

$$\text{yield}(\%) = \frac{n_{C_3H_6}}{n_{C_3H_8} + n_{C_3H_6} + ((2/3) \times n_{C_2H_6}) + ((2/3) \times n_{C_2H_4}) + ((1/3) \times n_{CH_4})} \times 100\%$$

$$\text{selectivity}(\%) = \frac{(a_i/3)n_i}{n_{C_3H_6} + ((2/3) \times n_{C_2H_6}) + ((2/3) \times n_{C_2H_4}) + ((1/3) \times n_{CH_4})} \times 100\%$$

$$\text{conversion}(\%) = \frac{\text{yield}(\%)}{\text{selectivity}(\%)} \times 100\%$$

where F_p is the moles of propane fed per second, C_p is the conversion of propane per gram of the catalyst, a_i and n_i are the number of carbon atoms in the product and their moles, respectively.

The calculations did not take into account the conversion of propane to coke, because its instantaneous formation is time dependent and difficult to estimate. The coke amount was estimated independently from the amounts of CO and CO_2 evolved during oxidative regeneration of the catalysts. In these experiments after 480 min-on-stream the catalyst was heated in dry air at the rate 15 °C min^{-1} from room temperature to the final temperature of 600 °C. The evolved carbon oxides were analyzed by GC equipped with TCD detector. These results indicate that in all process the total percent of propane converted to coke not exceeds 0.5%.

2.4. In situ UV–vis DR study

During the dehydrogenation of propane with CO_2 over Cr3.4/SBA-1 catalyst the oxidation state of chromium species was monitored by UV–vis DR spectroscopy using Ocean Optics HR2000+ instrument (integration time 20 ms, 20 scans) equipped with Ocean Optics DH-2000 BAL halogen–deuterium light source and a high temperature reflection probe (FCR-7UV400-2-ME-HTX, 7 × 400 μm fibers). The probe was attached at the top of modify quartz microreactor within the distance of 2–3 mm from catalyst bed. The spectra were collected in the range between 250 and 1050 nm with interval 2 s.

3. Results and discussion

3.1. Characterization of supports

Two commercial silica gels, SiO_2-p (Polish Chemical Reagents) and SiO_2-a (Aldrich), as well as mesoporous sieves with hexagonal (SBA-15) and cubic (SBA-1) pore structures were applied as the supports. The structure and morphology of pure SBA-1 and

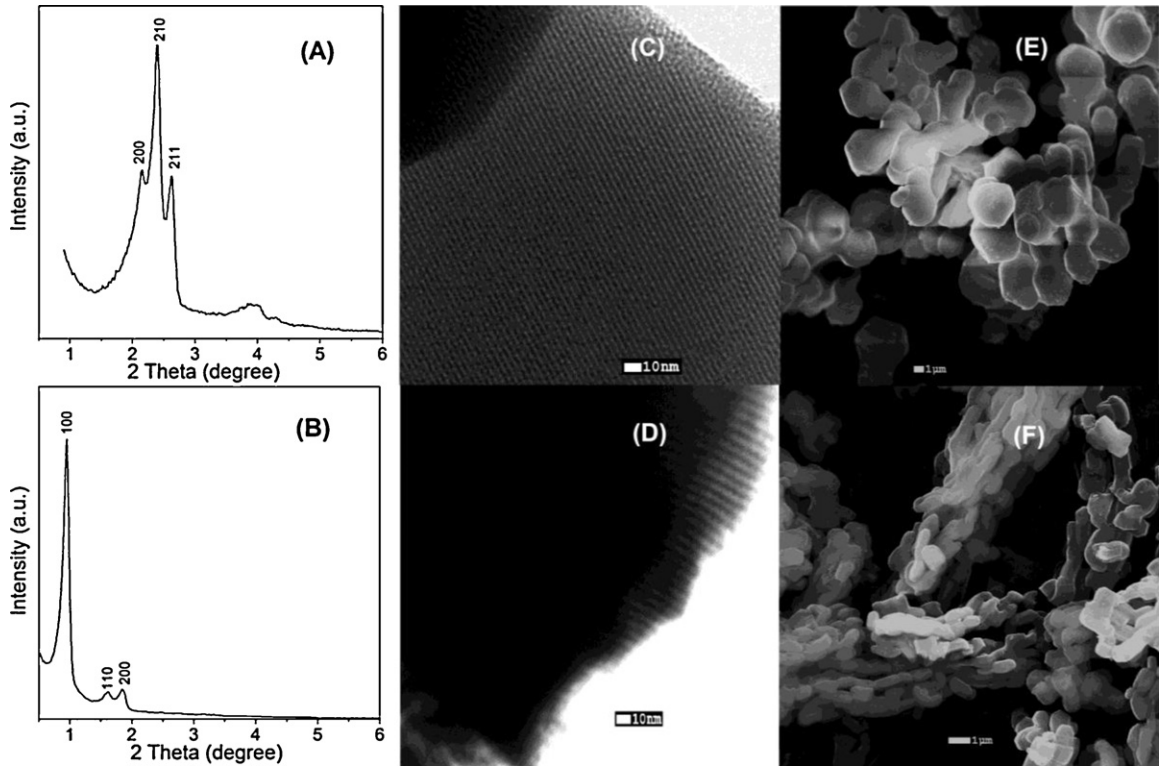

Fig. 1. Low angle X-ray diffractograms, TEM and SEM images of SBA-1 (A, C and E) and SBA-15 (B, D and F).

SBA-15 were investigated with X-ray diffraction, TEM and SEM analysis (Fig. 1(A–F)).

The diffraction patterns of both mesoporous samples show three well-resolved peaks indicating long-range structural order also confirmed by TEM analysis (Fig. 1(C and D)). The XRD pattern of SBA-1 shows (2 1 0), (2 0 0) and (2 1 1) reflections characteristic for the cubic phase, which is indexed to the Pm3n space group [43]. In the case of SBA-15, the diffraction peaks can be indexed as (1 0 0), (1 1 0) and (2 0 0) reflections associated with the hexagonal P6mm space symmetry [44]. Furthermore, the SEM images reveal that both materials consist of aggregated microparticles (Fig. 1(E and F)). SBA-1 has a branch-like structure, composed of spherical particles sized of 2–5 μm which are linked with each other, while SBA-15 consists of wheat-like aggregates with rope-like domains with a uniform size of 1–2 μm.

Nitrogen adsorption–desorption isotherms of the supports are presented in Fig. 2(A). All of the silica materials exhibit type IV isotherms according to IUPAC classification. The isotherms of SBA-15, SiO_2-a and SiO_2-p show H1 type hysteresis loop that is attributed to mesoporous materials with cylindrical pores and a narrow pore size distribution, while SBA-1 do not exhibit a hysteresis loop, which is characteristic for a capillary condensation in 3-D materials with a small cage-type porous structure [45,46].

Fig. 2(B) shows the distribution of the pore size calculated from the adsorption branch of isotherms with the use of the BJH method. Commercial silica materials, SiO_2-a and SiO_2-p, exhibit a broad pore distribution in the range of 2–13 nm, while SBA-1 and SBA-15 mesoporous sieves show a uniform pore size in the narrow range of 2–4 nm and 4–8 nm, respectively.

The textural and structural parameters of the supports, obtained from the low-temperature nitrogen adsorption isotherms and from XRD patterns, are summarized in Table 1.

It is clear that all of the materials strongly differ in the specific surface area that decreases in the following order: SBA-1 > SBA-15 > SiO_2-a > SiO_2-p. The S_{BET} of SBA-1 is approximately 4.5 times higher than that of SiO_2-p. In contrast, the pore volume changes in a relatively narrow range between 0.70 and 0.92 $cm^3\ g^{-1}$.

3.2. Base catalysts' characterization

3.2.1. Cr surface composition over various siliceous supports

The presence of Cr^{6+} and Cr^{3+} species in the calcined catalysts was investigated with UV–vis DR spectroscopy (Fig. 3(A–D)).

In all of the spectra, two intensive absorption bands at 270 and 360 nm dominate. They originate from $O \rightarrow Cr^{6+}$ charge transfer transitions of chromate species. Particularly, the bands at 270 nm and 360 nm are the results of the transfer transitions $^1A_1 \rightarrow {}^1T_2$ ($1t_1 \rightarrow 7t_2$ and $6t_2 \rightarrow 2e$) and $1A_1 \rightarrow 1T_2$ ($1t_1 \rightarrow 2e$), respectively [31,48]. An additional shoulder band at about 455 nm, typical for dichromates [49], is also present and its intensity rises gradually with the total Cr content indicating an increase in the polymerization degree of the Cr^{6+} species. Moreover, the latter band shifts slightly to a higher wavelength and becomes more asymmetric with the increasing Cr_{tot} content. This suggests that at a higher content, the band characteristic for dichromates (455 nm) overlaps with the weak band characteristic for the d–d transition of Cr^{3+} ($A_{2g} \rightarrow T_{1g}$) located at about 465 nm. The presence of the Cr^{3+} species in the samples with a higher Cr_{tot} content also confirms the appearance

Table 1
The textural and structural parameters of supports.

Support	S_{BET} ($m^2\ g^{-1}$)	Pore volume ($cm^3\ g^{-1}$)	a_0 (nm)[a]
SBA-1	1181	0.70	8.10
SBA-15	750	0.89	10.4
SiO_2-a	477	0.92	–
SiO_2-p	261	0.71	–

[a] The lattice parameters a_o of SBA-1 and SBA-15 materials were calculated based on the formulas: $a_0 = d_{2\,1\,0}\sqrt{5}$ and $a_0 = 2d_{1\,0\,0}/\sqrt{3}$, respectively [47].

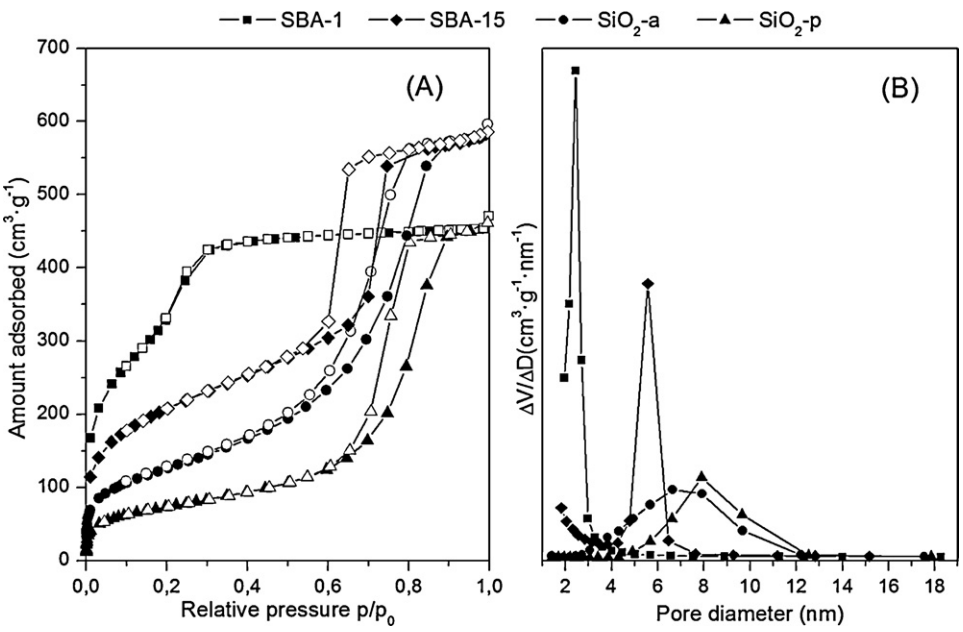

Fig. 2. Nitrogen adsorption–desorption isotherms (A) and BJH mesopore size distributions (B) of the silica suppots.

of a new broad band located at about 600 nm that is due to d–d transitions of Cr^{3+} ($A_{2g} \rightarrow T_{2g}$) in octahedral symmetry like in Cr_2O_3. The latter absorption band is present in the spectra of the Cr*x*/SiO_2-p, Cr*x*/SiO_2-a and Cr*x*/SBA-15 catalysts with 2.1, 3.4 and 6.8 wt.% of Cr, while in the case of the Cr*x*/SBA-1 series, the band at 600 nm appears only in the spectrum of the sample with the highest Cr content (Cr6.8/SBA-1). Moreover, in the Cr*x*/SiO_2-p, Cr*x*/SiO_2-a and Cr*x*/SBA-15 series, the intensity of the 600 nm band increases gradually with the increase of the Cr content, indicating that the Cr^{3+} species are produced after exceeding the monolayer coverage of the support.

The presence of the Cr^{3+} species in the catalysts with high Cr loadings was confirmed with XRD (Fig. 4). In the 2 Theta range of 5–70° the diffraction lines corresponding to the crystal phase of α-Cr_2O_3 were detected. These lines are presented in the XRD patterns of all catalysts with the highest Cr content. They were also observed in the patterns of Cr3.4/SiO_2-p, Cr3.4/SiO_2-a, Cr3.4/SBA-15 and in Cr2.1/SiO_2-p samples. However, a comparison of UV–vis DRS with

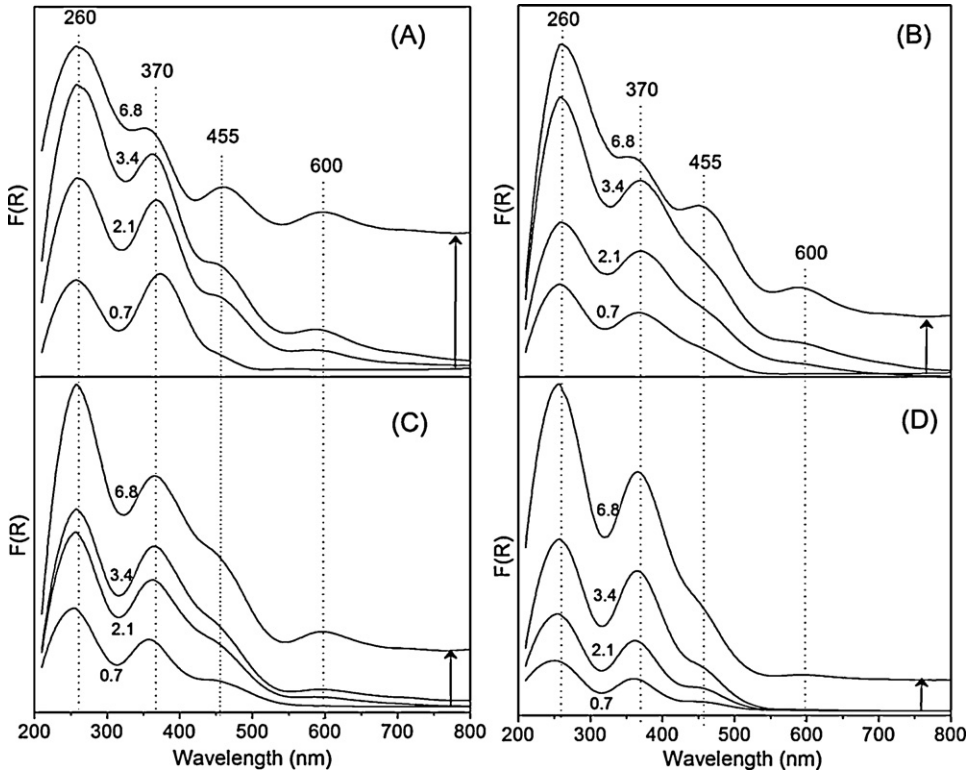

Fig. 3. UV–vis diffuse reflectance spectra of fresh Cr*x*/SiO_2-p (A), Cr*x*/SiO_2-a (B), Cr*x*/SBA-15 (C) and Cr*x*/SBA-1 (D) catalyst series with increasing Cr content. The values: 0.7, 2.1, 3.4 and 6.8 indicate wt.% of Cr. For clarity, the spectra of the catalysts with the highest Cr content were shifted vertically.

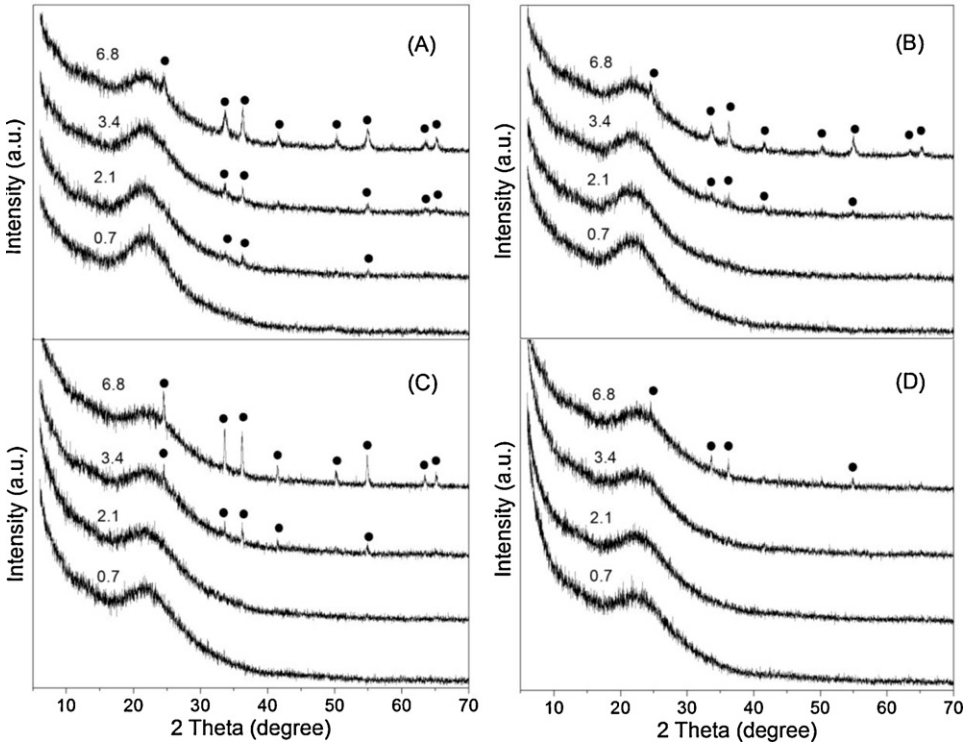

Fig. 4. X-ray diffractograms measured for fresh Cr*x*/SiO_2-p (A), Cr*x*/SiO_2-a (B), Cr*x*/SBA-15 (C) and Cr*x*/SBA-1 (D) catalyst series with increasing Cr content. The values: 0.7, 2.1, 3.4 and 6.8 indicate wt.% of Cr. For clarity, the curves have been shifted vertically by 300 counts. Peaks of α-Cr_2O_3 are marked with symbol "●".

the XRD results reveals that the lines of α-Cr_2O_3 were absent in the patterns of Cr2.1/SiO_2-a and Cr2.1/SBA-15. In this case, the weak absorption band at 600 nm was found with UV–vis DRS. This may be explained either by high dispersion or by a smaller size of Cr_2O_3 crystals. However, XRD is not a sensitive technique, therefore we cannot exclude that the absence of the patterns corresponding to α-Cr_2O_3 is due to the detection limit of this technique.

In the case of silica-supported chromium oxide materials, crystalline Cr_2O_3 particles are detected at relatively low Cr contents in comparison to other supports, such as Al_2O_3 and ZrO_2. For example, Gaspar et al. [29] have detected crystalline Cr_2O_3 in the Cr/SiO_2 samples with the Cr content of 1.5 wt.%, while McDaniel and Welch [50] observed that Cr_2O_3 was formed starting from 2.9 wt.% of Cr. Other authors observed the formation of agglomerated Cr_2O_3 species even in Cr/SiO_2 samples with less than 1.5 wt.% of Cr [32,51]. Such tendency to form Cr_2O_3 clusters, rather than a well-dispersed phase, is due to a low concentration of reactive hydroxyl groups on the silica surface. Our XRD results indicate that in the group of catalysts obtained with the same procedure (preparation conditions, precursor, etc.) the formation of crystalline Cr_2O_3 depends on the silica support's properties. The specific surface area of the support is important to maintain a high dispersion of chromium species. In the case of the SiO_2-p support which has the lowest surface area (S_{BET} = 261 $m^2\ g^{-1}$), crystalline Cr_2O_3 appeared in the samples starting from 2.1 wt.% of Cr, while over SiO_2-a which has a moderate specific surface area (S_{BET} = 477 $m^2\ g^{-1}$) crystalline Cr_2O_3 was detected with XRD above 3.4 wt.% of Cr. At a similar total Cr content, the Cr_2O_3 particles appear over SBA-15-supported materials (S_{BET} = 750 $m^2\ g^{-1}$). The latter results are in good agreement with the recent report of Zhang et al. [52]. On the basis of Raman, XPS, XRD and UV–vis DRS studies it has been estimated that in the case of the CrO_x/SBA-15 catalysts (S_{BET} = 796 $m^2\ g^{-1}$ of SBA-15 support), obtained with the impregnation method, agglomerated Cr^{3+} species appear above 3.6 wt.% of Cr (Cr surface density 0.54 Cr-at. nm^{-2}). In contrast, over the SBA-1 support that has the highest surface area (S_{BET} = 1181 $m^2\ g^{-1}$), α-Cr_2O_3 particles were found only in the Cr6.8/SBA-1 sample. Similarly to our previous investigations, concerning Cr/MCM-41 systems (S_{BET} = 997 $m^2\ g^{-1}$ of MCM-41 support), crystalline Cr_2O_3 was detected with XRD in the samples with the Cr content above 6.8 wt.% [3].

Table 2 summarizes the quantitative results of the fresh catalysts characterization. Based on ICP, chemical analysis with Bunsen–Rupp method and S_{BET} measurements the percent concentration and surface density of Cr^{6+} species in the fresh catalysts were determined.

In the case of the Cr*x*/SiO_2-a, Cr*x*/SBA-15 and Cr*x*/SBA-1 catalysts, the content of the Cr^{6+} species increases gradually with the increase of Cr_{tot} loading, while in the Cr*x*/SiO_2-p series, the maximum Cr^{6+} content is reached in the Cr3.4/SiO_2-p catalysts. In the latter case, the Cr^{6+} content is 1.19 wt.% (0.61 Cr^{6+} ions nm^{-2}) what is in agreement with the results of Hakuli et al. [32] who reported 1.03 wt.% for a similar catalytic system (using SiO_2 with S_{BET} = 317 $m^2\ g^{-1}$). Furthermore, on the basis of the amount of Cr_{tot} and the Cr^{6+} species concentration, the fraction of the Cr^{3+} species oxidized to Cr^{6+} was calculated (the last column in Table 2). In all of the catalysts' series, the highest fraction of chromium stabilized as the Cr^{6+} species is obtained at the lowest Cr_{tot} content. The Cr^{6+}/Cr_{tot} ratio decreases with the increase of the Cr content, however detailed behaviour varies with the type of the support. In the case of the Cr*x*/SBA-1 and Cr*x*/SBA-15 series the Cr^{6+}/Cr_{tot} ratio remains almost constant at medium Cr_{tot} contents, while it decreases at the highest contents. In contrast in the Cr*x*/SiO_2-a and Cr*x*/SiO_2-p series the increase of Cr_{tot} always leads to a decrease of the Cr^{6+}/Cr_{tot} ratio.

The chemical analysis' results are in good agreement with the UV–vis DR spectroscopic and XRD data. All these techniques confirm that at low loadings (below monolayer coverage of the support) the Cr^{6+} species are dominant, whereas, above the monolayer coverage, Cr^{6+} and agglomerated Cr^{3+} species (amorphous or crystalline Cr_2O_3) coexist. Moreover, it is clear that the application of

Table 2
Base characterization results of the fresh catalysts.

Catalyst	S_{BET} ($m^2\ g^{-1}$)	Cr_{tot} (Cr wt.%)[a]	Cr^{6+} amount		Cr^{6+}/Cr_{tot} (%)
			(Cr^{6+} wt.%)[b]	(Cr^{6+} ions nm^{-2})[c]	
Cr0.7/SBA-1	1108	0.73	0.60	0.06	82
Cr2.1/SBA-1	1079	2.32	1.62	0.17	70
Cr3.4/SBA-1	962	3.87	2.81	0.32	73
Cr6.8/SBA-1	810	6.88	4.43	0.63	64
Cr0.7/SBA-15	737	0.77	0.58	0.09	76
Cr2.1/SBA-15	633	2.40	1.49	0.27	62
Cr3.4/SBA-15	526	3.47	2.23	0.49	64
Cr6.8/SBA-15	446	6.72	2.69	0.70	40
Cr0.7/SiO_2-a	469	0.82	0.56	0.14	68
Cr2.1/SiO_2-a	420	2.39	1.23	0.34	52
Cr3.4/SiO_2-a	404	3.66	1.67	0.48	46
Cr6.8/SiO_2-a	380	6.97	1.91	0.58	27
Cr0.7/SiO_2-p	251	0.81	0.50	0.23	62
Cr2.1/SiO_2-p	234	2.34	1.17	0.58	50
Cr3.4/SiO_2-p	225	3.54	1.19	0.61	33
Cr6.8/SiO_2-p	201	6.93	1.02	0.59	15

[a] Determined by ICP.
[b] Determined with Bunsen–Rupp method.
[c] Cr^{6+} surface density, calculated using surface area of the catalysts.

the mesoporous materials with a high specific surface area, such as SBA-1, allows for a much higher fraction of the Cr^{6+} species at higher Cr_{tot} loadings than in the case of commercial silica gels or SBA-15 that has a much lower S_{BET}.

3.2.2. Catalysts' redox properties

Fig. 5 presents the temperature-programmed reduction profiles of the fresh catalysts.

In all of the profiles, the main reduction peak appears in the temperature range between 400 and 460 °C. This peak was assigned to the reduction of Cr^{6+} to Cr^{3+} or Cr^{2+} species directly attached to the silica materials [32]. Moreover, in all of the series of catalysts, the temperature maximum position shifts to lower values with the increase of the Cr content what can be attributed to the change in the polymerization degree of the Cr^{6+} species. Furthermore, in the profile of the catalysts with the highest Cr content (except for Cr6.8/SBA-1) an additional reduction peak at ca. 270–300 °C has appeared. The location of this peak coincides with low temperature reduction maximum observed for bulk α-Cr_2O_3, what is assigned to the reduction of Cr^{6+} to Cr^{3+} or Cr^{2+} species dispersed on α-Cr_2O_3 [3,32,53].

Quantitative information concerning the H_2-consumption was obtained from the TPR peak areas with an appropriate calibration of the TCD signal. Fig. 6(A and B) shows the variation of H_2-consumption with the Cr_{tot} and Cr^{6+} content as well as the expected H_2-consumption in Cr^{6+} reduction to Cr^{3+} and Cr^{2+} species (dot lines). The expected values were calculated with the assumption that all chromium species presented in the catalysts are stabilized as Cr^{6+} species and they are reduced selectively either to Cr^{3+} ($2CrO_3 + 3H_2 = Cr_2O_3 + 3H_2O$; $H_2/Cr = 1.5$) or to Cr^{2+} ($CrO_3 + 2H_2 = CrO_2 + 2H_2O$; $H_2/Cr = 2.0$) species.

Fig. 6(A) clearly shows that in the case of the catalysts with the lowest Cr_{tot} content, the H_2-consumption varies within a narrow range, close to the expected values. The differences between the expected and measured H_2-consumptions increase together with the rise of the Cr_{tot} content. This indicates that the fraction of nonredox Cr species increases rapidly above the monolayer coverage. Moreover, with the rise of the Cr_{tot} content, the difference in H_2-consumption between the catalysts series also increases. In the series of Cr*x*/SiO_2-p catalysts, the maximum H_2-consumption is obtained for the Cr2.1/SiO_2-p catalyst and then declines slightly for the catalysts with higher Cr contents, whereas in the case of Cr*x*/SiO_2-a, Cr*x*/SBA-15 and Cr*x*/SBA-1 series, the rise of Cr_{tot} content (in the investigated range) always leads to an increase of the H_2-consumption. However, the H_2-consumption increases more sharply in the case of Cr*x*/SBA-1 series than in the case of Cr*x*/SBA-15 and Cr*x*/SiO_2-a series, what indicates that SBA-1 may stabilize a much bigger number of Cr^{6+} species than the other investigated supports.

Fig. 6(B) shows the relation between the H_2-consumption and the Cr^{6+} species content in fresh catalysts determined with the Bunsen–Rupp method. In all of the cases the H_2-consumption varies within the range of the expected values for Cr^{6+} reduction to Cr^{3+} and Cr^{2+} species what indicates that both of the species exist in the H_2-reduced catalysts. Additionally, the variations of H_2/Cr^{6+} ratio with the Cr_{tot} content are presented in Fig. 6(B) (inset). In all of the catalyst series, the ratio of H_2/Cr^{6+} decreases gradually with the increase of the Cr_{tot} content. For catalysts with the lowest Cr_{tot} content (~0.7 wt.%) the ratios of H_2/Cr^{6+} are in the range of 2.0–1.9 what indicates a deep reduction of Cr^{6+} to Cr^{2+} species, whereas at the highest Cr_{tot} content the ratios decrease to 1.55–1.75 proving a formation of Cr^{3+} together with Cr^{2+} species. A similar variation between the total Cr content in the catalyst and the concentration of Cr^{2+} and Cr^{3+} species in catalysts reduced with CO or H_2 has been previously reported [31,32]. It has been proposed that the Cr^{2+}/Cr^{3+}ratio is strongly influenced by chromium dispersion. At a low Cr content, where a high dispersion is expected, Cr^{3+} species migration to stable Cr_2O_3 clusters is slow, therefore Cr^{3+} may be further reduced to Cr^{2+}. However, at a high Cr content the dispersion is lower, therefore the reduction stops at Cr_2O_3 [31].

3.3. Dehydrogenation of propane with carbon dioxide

Table 3 summarizes the initial results of catalytic tests obtained in the dehydrogenation of propane with CO_2 (DHP–CO_2) over the catalysts containing ~3.4 wt.% at 550 °C.

The initial reaction rate normalized per catalyst weight (activity), carbon dioxide and propane conversions decrease in the following order: Cr3.4/SBA-1 > Cr3.4/SBA-15 > Cr3.4/SiO_2-a > Cr3.4/SiO_2-p indicating clearly that Cr dispersion is crucial for high activity.

Over the catalysts containing ~3.4 wt.% of Cr, the main product is propene, which is produced with high selectivity (88–93%). Additionally, light hydrocarbons (methane, ethene and ethane), formed probably in the cracking and hydrocracking reactions, as well as H_2, CO and H_2O were found in the products.

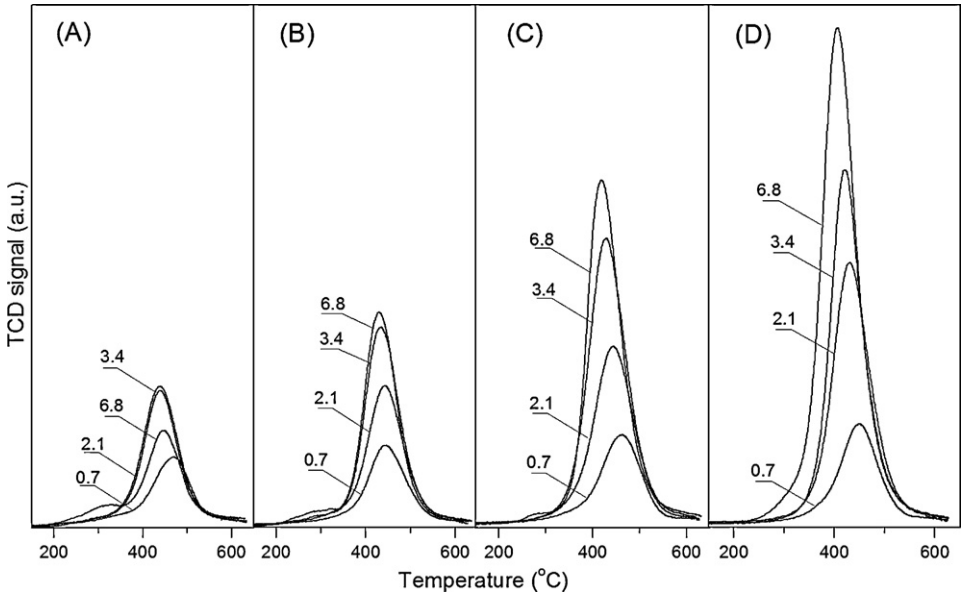

Fig. 5. H_2-TPR profiles of fresh Cr*x*/SiO_2-p (A), Cr*x*/SiO_2-a (B), Cr*x*/SBA-15 (C) and Cr*x*/SBA-1 (D) catalyst series. The values: 0.7, 2.1, 3.4 and 6.8 indicate wt.% of Cr.

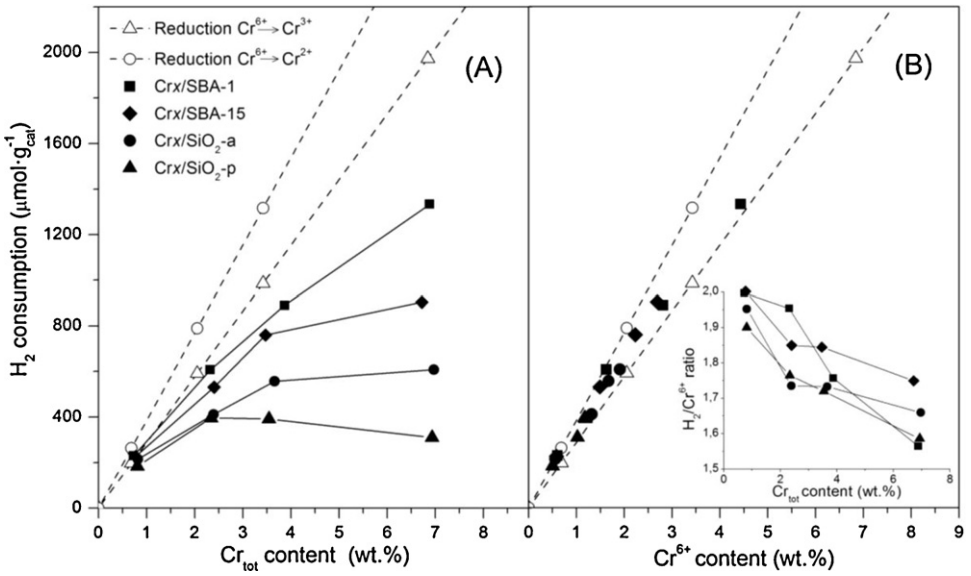

Fig. 6. Variation of hydrogen consumption with Cr_{tot} (A) and Cr^{6+} (B) species content in the fresh catalysts as well as the ratio of H_2/Cr^{6+} with the Cr_{tot} (inset). Dot line represents the theoretical H_2 consumptions for selective Cr^{6+} reduction to Cr^{2+} and Cr^{3+} species.

The primary recourses of CO in the DHP–CO_2 process are oxidative dehydrogenation of propane with CO_2 (1) and reverse water-gas shift reactions (2), while H_2 is mainly produced in dehydrogenation reaction (3). Taking to assume the above reactions sum of H_2 and CO moles produced in the DHP–CO_2 process should be equal to propene moles and the molar ratio of $(CO + H_2)/C_3H_6$ should be equal to one. It is clear from the Table 3 that the initial molar ratios of the primary products $(CO + H_2)/C_3H_6$ are higher (1.3–1.5) indicating side reactions contribution. Over the investigated catalysts the ratio of $(CO + H_2)/C_3H_6$ drops gradually during the 100 min-on-stream and then remains almost constant at a level 1.1–1.2. This indicates that at steady state conditions the main

Table 3
Catalytic performance of silica-supported materials containing ~3.4 wt.% of Cr at 550 °C.[a]

Catalyst	Activity ($mol_{C_3H_8}\,s^{-1}g^{-1}$) ($\times 10^6$)	Conversion (%)		Selectivity (%)				Molar ratio (mol mol^{-1})	
		C_3H_8	CO_2	C_3H_6	C_2H_6	C_2H_4	CH_4	$(CO + H_2)/C_3H_6$	CO/H_2
Cr3.4/SBA-1	2.6	33.2	4.6	87.9	2.9	3.3	5.9	1.5 (1.2)[b]	1.0 (0.8)
Cr3.4/SBA-15	2.2	27.2	3.4	89.3	2.4	3.5	4.7	1.4 (1.1)	0.9 (0.8)
Cr3.4/SiO_2-a	1.6	23.2	3.3	90.3	1.7	3.1	4.9	1.4 (1.1)	1.2 (0.9)
Cr3.4/SiO_2-p	1.2	15.4	2.1	92.6	1.3	2.5	3.6	1.3 (1.1)	1.1 (0.7)

[a] Reaction conditions: CO_2:C_3H_8:He molar ratio = 5:1:9; total flow rate = 30 cm^3 min^{-1}; catalyst weight = 200 mg; reaction time = 10 min.
[b] The values in the brackets are calculated after 460 min on-stream.

resources of the primary products in DHP–CO_2 are the mentioned above three reactions. Based on these results we cannot indicate the pathway of CO formation, because it can be produced simultaneously both in the (1) and (2) reactions. However, taking to assume that the values of $(CO + H_2)/C_3H_6 \cong 1$ and the ratios of CO/H_2 (the last column in Table 3) we can softly estimate that at steady sate not less than 50% of propene is produced by dehydrogenation of propane reaction.

Fig. 7(A) shows the variation between the Cr_{tot} content in the four series of catalysts and the initial rate of propene formation in the DHP–CO_2 at 550 °C.

In the presence of catalysts with comparable Cr_{tot} contents, the rate of propene formation decreases in the following order: Cr*x*/SBA-1 > Cr*x*/SBA-15 > Cr*x*/SiO_2-a > Cr*x*/SiO_2-p. Moreover, in the particular series of catalysts, the rate of propene formation increases steeply with the increase of the Cr_{tot} content to about 2.1 wt. % in the Cr*x*/SiO_2-p series and to about 3.4 wt.% in the other series. After exceeding the mentioned contents of Cr_{tot}, the rate either decreases as in the Cr*x*/SiO_2-p and Cr*x*/SiO_2-a series or only slightly rises as in the other investigated series of catalysts.

The above described variation between Cr_{tot} content and propene formation rate can be explained based on the characterization results. The unfavourable effect observed at high Cr_{tot} contents is a result of less/no active crystalline α-Cr_2O_3 formation which is created after exceeding the monolayer coverage of the support. It is clear from Fig. 7(B) that in all series of catalysts the rate increases clearly until the Cr_{tot} content density not exceed about 1 Cr at. nm^{-2}. XRD results (Fig. 4(A–D)) proved that the particles of α-Cr_2O_3 are presented in all the catalysts with Cr_{tot} surface density at and above 1 Cr at. nm^{-2}.

On the other hand, high activity is related to dispersed species. The characterization results indicate that on the surface of all fresh catalysts dominate Cr^{6+} species. The H_2-TPR quantitative measures (Fig. 5(A)) and titrations performed for fresh catalysts with the use of the Bunsen–Rupp method (Table 2), proved that the concentration of Cr^{6+} species in the catalysts changes, depending on the support properties and Cr_{tot} loading, in a way similar to the rate of propene formation in the dehydrogenation of propane with CO_2 (Fig. 7(A)). A clear proportion between the content of the precursor of active sites (Cr^{6+} species) in calcined catalysts and the rate of propene formation is presented in Fig. 7(C). Regardless to the siliceous support used, the rate increases together with the increase of the Cr^{6+} content in the fresh catalysts.

In the case of silica-supported chromium oxide catalysts, it has been revealed that highly dispersed, coordinately unsaturated Cr^{3+} and/or Cr^{2+} sites are responsible for the activity in the process of nonoxidative dehydrogenation of hydrocarbons [32,39,54]. These sites are created in the initial stage of the process as a result of reduction with the substrates (hydrocarbons) of the dispersed Cr^{6+} species present on the surface of fresh or regenerated with air catalysts. In the DHP–CO_2 the primary role of Cr^{6+} species is similar as in the nonoxidative reaction. E.g. Cr^{6+} species present in the fresh or regenerated catalysts are precursors of highly dispersed Cr^{3+} and Cr^{2+} species which exhibit a high activity in the nonoxidative pathway of propene formation.

It should be also pointed that in the presence of CO_2 propene can be produced not only by nonoxidative dehydrogenation but also by the oxidative dehydrogenation pathway (reactions (4) and (5)). In such redox cycle may participates Cr^{6+} species are reduced to Cr^{3+} species by hydrocarbons (4) and, inversely, the Cr^{3+} species are oxidized with CO_2 (5) [12,55].

$$3R\text{–}CH_2\text{–}CH_3 + 2CrO_3 \leftrightarrows 3R\text{–}CH{=}CH_2 + Cr_2O_3 + 3H_2O \quad (4)$$

$$3CO_2 + Cr_2O_3 \leftrightarrows 3CO + 2CrO_3 \quad (5)$$

Table 4
The deactivation data.

Catalyst	Activity loss ($mol_{C_3H_8}\,s^{-1}g^{-1}$) ($\times 10^6$)	Coke (mg)	$n_{C(coke)}/n_{C(propane)}$ (%)[a]
Cr3.4/SBA-1[b]	1.1	5.8	0.38
Cr3.4/SBA-15[b]	0.9	3.7	0.24
Cr3.4/SiO_2-a[b]	0.7	3.5	0.22
Cr3.4/SiO_2-p[b]	0.4	1.6	0.11
Cr3.4/SiO_2-p[c]	1.3	5.1	0.31
Cr3.4/SiO_2-p[d]	1.0	6.4	0.42

[a] Number of carbon atoms in the deposited coke per number of carbon atoms in the propane injected into the reactor during 480 min on-stream.
Dehydrogenation conditions:
[b] T_r = 550 °C; catalyst weight = 200 mg; CO_2:C_3H_8:He molar ratio = 5:1:9; total flow rate = 30 $cm^3\,min^{-1}$.
[c] T_r = 650 °C; catalyst weight = 200 mg; CO_2:C_3H_8:He molar ratio = 5:1:9; total flow rate = 30 $cm^3\,min^{-1}$.
[d] T_r = 550 °C; catalyst weight = 480 mg; CO_2:C_3H_8:He molar ratio = 5:1:9; total flow rate = 30 $cm^3\,min^{-1}$.

Taking the above into account, the behaviour of the Cr^{6+} species during dehydrogenation with CO_2 was monitored with UV–vis diffuse reflectance spectroscopy. Fig. 8(A–D) summarizes the *in situ* UV–vis DRS results collected during the initial 10 min of propane dehydrogenation with CO_2 over Cr3.4/SBA-1 catalyst at 550 °C.

Two intensive bands characteristic for $O \rightarrow Cr^{6+}$ charge transfer of chromates (at 260 nm and 370 nm) disappear in the first minute of the process, while at the same time a new band around 700 nm appears. The latter band is a superposition of two bands characteristic for pseudo-tetrahedral Cr^{2+} ($^5T_g \rightarrow {}^5E_{2g}$) and pseudo-octahedral $Cr^{2+/3+}$ ($^5T_g \rightarrow {}^5E_{2g}/{}^4T_g \rightarrow {}^4E_{2g}$) transitions and it indicates the presence of $Cr^{3+/2+}$ species in the reduced catalysts [49]. From the above experiment it is clear that the potentially active in oxidative dehydrogenation Cr^{6+} species, present in the calcined catalyst, are unstable under the dehydrogenation of propane with CO_2 reaction conditions. The Cr^{6+} species are rapidly reduced to Cr^{3+} and Cr^{2+} species at the beginning of the process what indicates that CO_2 is not an effective oxidation agent and under the reaction conditions cannot stop the Cr^{6+} species' reduction. This conclusion is in agreement with our and other researchers' observations according to which CO_2 exerts a very small oxidative effect during the regeneration of reduced catalysts with hydrogen or hydrocarbons [3,9,12].

To summarize, we can conclude that the proportion between the catalytic performances and the concentration of the Cr^{6+} species reported in Fig. 7(C) is due to the fact that these species are the precursors of the dispersed Cr^{3+} and Cr^{2+} sites which have a high activity in the nonoxidative dehydrogenation of propane. However, the *in situ* UV–vis DR experiment did not exclude an oxidative pathway of propene formation. Both, the *in situ* UV–vis DR and quantitative H_2-TPR results indicate that the Cr^{2+} and Cr^{3+} species exist in the reduced catalysts. In the presence of CO_2, these species may participate in a redox cycle. Such oxidation–reduction cycles between Cr^{3+} and Cr^{2+} species have been reported in many reactions including the oxidative dehydrogenation of ethylbenzene with CO_2 as well as the reverse water-gas shift reaction [56,57].

The variation of catalytic performances of the Cr3.4/SBA-1, Cr3.4/SBA-15, Cr3.4/SiO_2-a, and Cr3.4/SiO_2-p catalysts with the time-on-stream (TOS) is presented in Fig. 9. Additional data concerning activity loss defined as the difference between the initial (after 10 min on-stream) and final (after 460 min on-stream) activity as well as the coke amount estimated after 480 min on-stream are summarized in Table 4.

All of the catalysts exhibit a similar behaviour during the process. The activity decreases gradually with the TOS while the selectivity to propene increases steeply between the 1st and

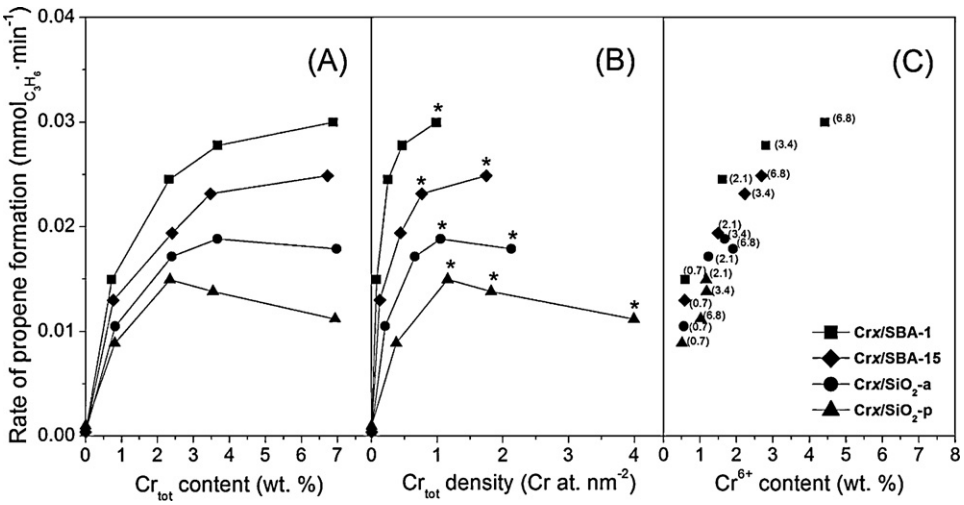

Fig. 7. Variation of propene formation rate with Cr_{tot} content (A), Cr_{tot} density (B) and Cr^{6+} species content (C) in the calcined catalysts. The values in the brackets in (C) indicate wt.% of Cr_{tot}. Reaction conditions: T_r = 550 °C; CO_2:C_3H_8:He molar ratio = 5:1:9; total flow rate = 30 cm^3 min^{-1}; catalyst weight = 200 mg; reaction time = 10 min; (*) indicates the catalysts in which the crystalline Cr_2O_3 was detected by XRD.

100th min of the process and then after it increases only slightly with TOS.

In the case of silica-supported chromium oxide catalysts the deactivation can be caused by several reasons, like inactive Cr species formation or coke deposition. In the case of Cr*x*/SBA-1 and Cr*x*/SBA-15, the destruction of mesoporous rearrangement could be an additional reason. However, our previous investigation concerning Cr-SBA-1 systems obtained with direct methods indicated that several dehydrogenation-regeneration cycles lead to a small, irreversible deactivation (deactivation that cannot be remove by oxidation in air) assigned either to inactive species formation or pores structure destruction [4]. This leads us to conclusion that the primary reason of deactivation under investigated conditions in the case of mesoporous catalysts (Cr3.4/SBA-1, Cr3.4/SBA-15) is coke deposition. In the case of Cr3.4/SiO_2-a, and Cr3.4/SiO_2-p catalysts we cannot exclude that additional reason is also deactivation by inactive Cr species formation as reported previous [12].

The comparison of the deactivation data summarized in Table 4 with the catalytic results presented in Fig. 9(A) indicates that the activity loss and the coke amount rise together with the increase of activity. Such a relation between the catalytic activity and the deactivation data can be explained in terms of the substrate–product reactivity. Several recent investigations have concluded that in the dehydrogenation with CO_2, coke is produced more intensively from unsaturated hydrocarbons than from the saturated ones [12,58]. Our results are in good agreement with that observation. The increase of propene concentration leads to an increase of mass of the created coke deposit. The preliminary formation of coke from propene in secondary reactions has been also confirmed with the *in situ* UV–vis DR investigation during nonoxidative dehydrogenation of propane. With the use a reactor system equipped with UV–vis diffuse reflectance probes (located at different catalyst bed heights). Nijhuis et al. [59] have shown that the coke formation rate is higher at the end of the catalyst bed, where the concentration of more reactive propene is higher.

Finally, in the case of the Cr3.4/SiO_2-p catalyst, the reaction conditions needed for obtaining the initial rate of propane formation similar to that over the Cr3.4/SBA-1 catalyst were

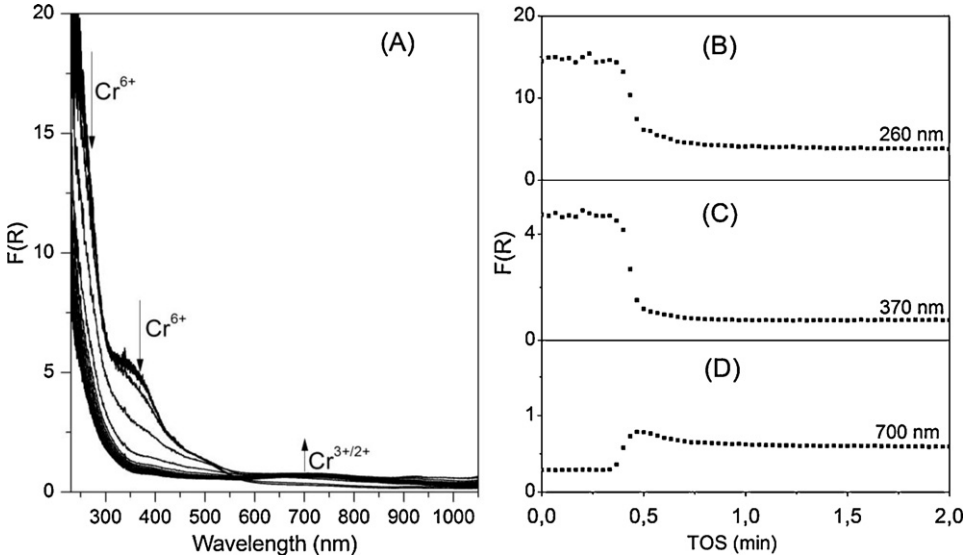

Fig. 8. *In situ* UV–vis DRS results recorded during initial step of propane dehydrogenation with CO_2 at 550 °C. (A) Spectra collected during first minute of process. (B–D) The variation of intensity of the band at 260 nm, 370 nm and 700 nm during 2 min on-stream. Reaction conditions: CO_2:C_3H_8:He molar ratio = 5:1:9; Total flow rate = 30 cm^3 min^{-1}; catalyst weight = 200 mg. The spectra were collected at regular interval 2 s.

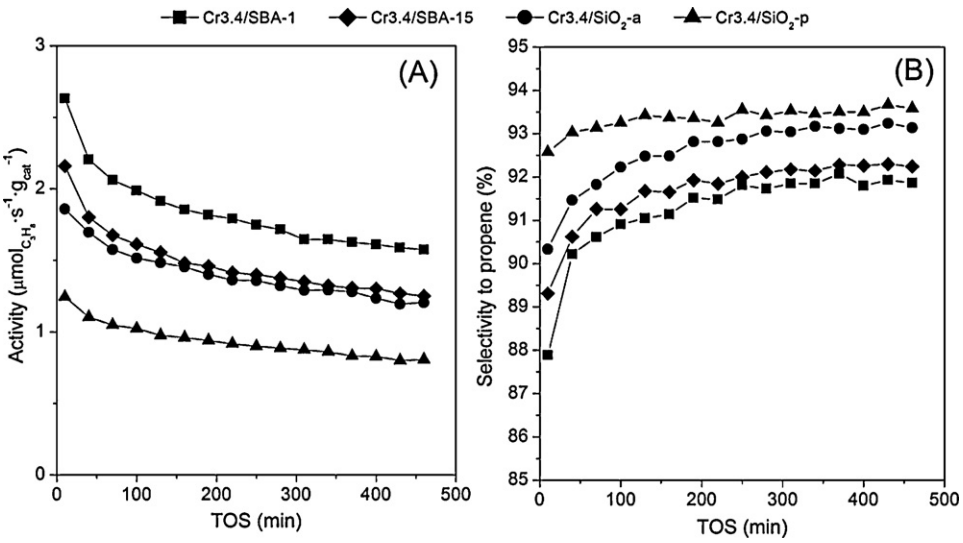

Fig. 9. Variation of activity (A) and selectivity to propene (B) with time-on-stream over selected catalysts. Reaction conditions: $T = 550\,^{\circ}C$; CO_2:C_3H_8:He molar ratio = 5:1:9; total flow rate = 30 $cm^3\ min^{-1}$; catalyst weight = 200 mg.

estimated (Fig. 10). This was achieved either by increasing the reaction temperature to 650 °C or by using a 2.4 times larger Cr3.4/SiO_2-p catalyst weight. The latter condition was estimated on the basis of the Cr^{6+} content in the calcined catalyst (the relation of the Cr^{6+} species' ratio in the Cr3.4/SBA-1 to that in the Cr3.4/SiO_2-p sample is 2.4), taking into account the correlation between catalytic performance and concentration of the Cr^{6+} species.

It is clear from Fig. 10 and Table 4 that over the Cr3.4/SiO_2-p catalyst the rise of propene formation rate by the increase of the reaction temperature leads to a faster deactivation by coke, whereas an increase of the catalyst weight (m_{cat} = 480 mg) leads to obtaining propene with a similar rate as over the Cr3.4/SBA-1 catalyst (m_{cat} = 200 mg). However, in the latter case the amount of coke and the number of propane molecules converted to coke were slightly higher. This might have been caused by a higher W/F factor. A longer contact time of the Cr3.4/SiO_2-p catalyst with more reactive propene favours formation of coke.

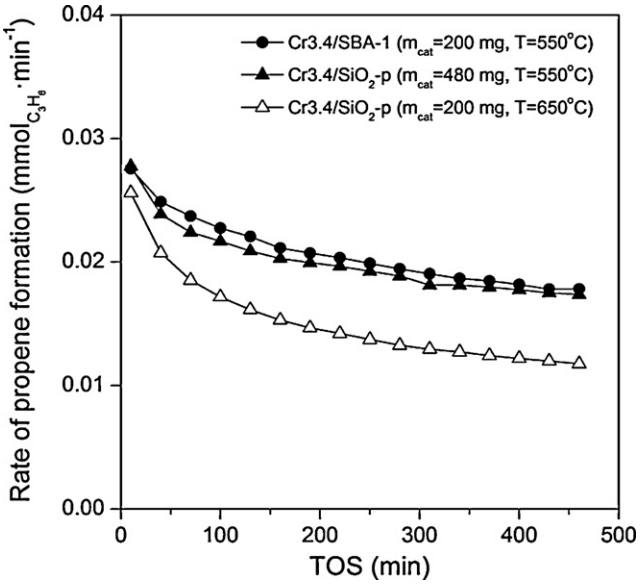

Fig. 10. Variation of propene formation rate with time-on-stream over Cr3.4/SiO_2-p and Cr3.4/SBA-1 catalysts at different reaction conditions. (△) $m_{cat.}$ = 480 mg. T_r = 550 °C. (▲) $m_{cat.}$ = 200 mg. T = 650 °C and (●) $m_{cat.}$ = 200 mg. T = 550 °C. In all cases, the CO_2:C_3H_8:He molar ratio = 5:1:9 and the total flow rate = 30 $cm^3\ min^{-1}$ were the same.

4. Conclusions

Four different series of silica supported chromium oxide-based catalysts varying in Cr content were prepared with the incipient wetness method, characterized with various techniques and tested in dehydrogenation of propane with CO_2. On the basis of the results, the following conclusions can be drawn:

- In terms of quality, similar types of Cr sites exist on the surface of the investigated materials. The Cr^{6+} species directly attached to the support dominate at a low total Cr content, whereas at a higher content, after exceeding monolayer coverage of supports, the particles of Cr_2O_3 are produced.
- The quantitative composition of the investigated materials strongly depends on the support's properties. The concentration of the Cr^{6+} species, the percentage of the Cr^{3+} species (precursor) oxidized to high valence states as well as the monolayer coverage, above which crystalline α-Cr_2O_3 is produced, depend on the support's properties, especially its specific surface area, e.g. SBA-1 which has a large specific surface area stabilizes more Cr^{6+} species than SBA-15 and commercial silica materials which have 2–4 times lower specific surface areas.
- A high number of Cr^{6+} species in the calcined catalysts is crucial for their high catalytic activity in the dehydrogenation of propane to propene with CO_2. In the presence of feed (propane + CO_2), the Cr^{6+} species are rapidly reduced to dispersed Cr^{2+} and Cr^{3+} species which exhibit a high catalytic performance. In the presence of CO_2, the dispersed Cr^{2+} and Cr^{3+} species may participate both in oxidative and nonoxidative dehydrogenation of propane.

Acknowledgements

The Authors thanks Dr D. Mucha and Dr M. Zimowska from Polish Academy of Science for XRD analysis and SEM images, respectively. This work was supported by the Ministry of Science and High Education (Grant Number N N205 107335).

References

[1] L. Liu, H. Li, Y. Zhang, Catal. Commun. 8 (2007) 565–570.
[2] M. Botavina, G. Martra, Y. Agafonov, N. Gaidai, N. Nekrasov, D. Trushin, S. Coluccia, A. Lapidus, Appl. Catal. A: Gen. 347 (2008) 126–132.
[3] P. Michorczyk, J. Ogonowski, P. Kuśtrowski, L. Chmielarz, Appl. Catal. A: Gen. 349 (2008) 62–69.
[4] P. Michorczyk, J. Ogonowski, M. Niemczyk, Appl. Catal. A: Gen. 374 (2010) 142–149.
[5] X. Zhang, Y. Yue, Z. Gao, Catal. Lett. 83 (2002) 19–25.
[6] P. Michorczyk, J. Ogonowski, React. Kinet. Catal. Lett. 78 (2003) 41–47.
[7] Y. Wang, Y. Ohishi, T. Shishido, Q. Zhang, W. Yang, Q. Guo, H. Wan, K. Takehira, J. Catal. 220 (2003) 347–357.
[8] I. Takahara, M. Saito, Chem. Lett. (1996) 973–974.
[9] I. Takahara, W. Chang, N. Mimura, M. Saito, Catal. Today 45 (1998) 55–59.
[10] K. Nakagawa, C. Kajita, N. Ikenaga, M. Nishitani-Gamo, T. Ando, T. Suzuki, Catal. Today 84 (2003) 149–157.
[11] Y. Wang, Y. Ohishi, T. Shishido, Q. Hang, K. Takehira, Stud. Surf. Sci. Catal. 146 (2003) 725–728.
[12] K. Takehira, Y. Ohishi, T. Shishido, T. Kawabata, K. Takaki, Q. Zhang, Y. Wang, J. Catal. 224 (2004) 404–416.
[13] M. Kocoń, P. Michorczyk, J. Ogonowski, Catal. Lett. 101 (2005) 53–57.
[14] D. Fox, E. Lee, M.-H. Rei, Ind. Eng. Chem. Prod. Res. Dev. 11 (1972) 444–446.
[15] P. Michorczyk, J. Ogonowski, Appl. Catal. A: Gen. 251 (2003) 425–433.
[16] B. Zheng, W. Hua, Y. Yue, Z. Gao, J. Catal. 232 (2005) 143–151.
[17] B. Xu, B. Zheng, W. Hua, Y. Yue, Z. Gao, J. Catal. 239 (2006) 470–477.
[18] M. Chen, J. Xu, Y.M. Liu, Y. Cao, H.Y. He, J.H. Zhuang, K.N. Fan, Catal. Lett. 124 (2008) 369–375.
[19] M. Chen, J. Xu, F.Z. Su, Y.M. Liu, Y. Cao, H.Y. He, K.N. Fan, J. Catal. 256 (2008) 293–300.
[20] H. Li, Y. Yue, C. Miao, Z. Xie, W. Hua, Z. Gao, Catal. Commun. 8 (2007) 1317–1322.
[21] Y. Ren, F. Zhang, W. Hua, Y. Yue, Z. Gao, Catal. Today 148 (2009) 316–322.
[22] P. Michorczyk, P. Kuśtrowski, L. Chmielarz, J. Ogonowski, React. Kinet. Catal. Lett. 82 (2004) 121–130.
[23] I. Takahara, M. Saito, M. Inaba, K. Murata, Catal. Lett. 102 (2005) 201–205.
[24] J. Ogonowski, E. Skrzyńska, Catal. Lett. 124 (2008) 52–58.
[25] M. Chen, J. Xu, Y. Cao, H.-Y. He, K.-N. Fan, J.-H. Zhuang, J. Catal. 272 (2010) 101–108.
[26] M. Chen, J. Xu, Y.-M. Liu, Y. Cao, H.-Y. He, J.-H. Zhuang, Appl. Catal. A: Gen. 377 (2010) 35–41.
[27] O. Krylov, A. Mamedov, S. Mirzabekova, Catal. Today 24 (1995) 371–375.
[28] O. Krylov, A. Mamedov, S. Mirzabekova, Ind. Eng. Chem. Res. 34 (1995) 474–482.
[29] A. Gaspar, J. Brito, L. Dieguez, J. Mol. Catal. A: Chem. 203 (2003) 251–266.
[30] W. Jóźwiak, I. Dalla Lana, J. Chem. Soc. Faraday Trans. 93 (1997) 2583–2589.
[31] B. Weckhuysen, R. Schoonheydt, J.-M. Jehng, I. Wachs, S. Cho, R. Ryoo, S. Kijlstra, E. Poels, J. Chem. Soc. Faraday Trans. 91 (1995) 3245–3253.
[32] A. Hakuli, M. Harlin, L. Backman, O. Krause, J. Catal. 184 (1999) 349–356.
[33] G. Wang, L. Zhang, J. Deng, H. Dai, H. He, Ch. Tong Au, Appl. Catal. A: Gen. 355 (2009) 192–201.
[34] D.S. Kim, J.-M. Tatibouet, I. Wachs, J. Catal. 136 (1992) 209–221.
[35] W. Jóźwiak, W. Ignaczek, D. Dominiak, T. Maniecki, Appl. Catal. A: Gen. 258 (2004) 33–45.
[36] J. Kim, R. Ryoo, Chem. Mater. 11 (1999) 487–491.
[37] M. Kruk, M. Jaroniec, R. Ryoo, J. Kim, Chem. Mater. 11 (1999) 2568–2572.
[38] B. Grzbowska, J. Słoczyński, R. Grabowski, K. Wcisło, A. Kozłowska, J. Stoch, J. Zieliński, J. Catal. 178 (1998) 687–700.
[39] S. De Rossi, M. Casaletto, G. Ferraris, A. Cimino, G. Minelli, Appl. Catal. A: Gen. 167 (1998) 257–270.
[40] B. Weckhuysen, R. Schoonheydt, Catal. Today 51 (1999) 223–232.
[41] J. Dereń, J. Haber, J. Słoczyński, Chem. Anal. 6 (1961) 659–662 (English).
[42] B. Grzybowska-Świerkosz, Elementy katalizy heterogenicznej, PWN, 1993.
[43] D. Zhao, J. Feng, Q. Huo, N. Melosh, G. Fredrickson, B. Chmelka, G. Stucky, Science 279 (1998) 548–552.
[44] Q. Huo, D. Margolese, G. Stucky, Chem. Mater. 8 (1996) 1147–1160.
[45] P. Srinivasu, A. Vinu, Chem. Eur. J. 14 (2008) 3553–3561.
[46] V. Balasubramanian, C. Anand, R. Pal, T. Mori, W. Böhlmann, K. Ariga, A. Tyagi, A. Vinu, Micropor. Mesopor. Mater. 121 (2009) 18–25.
[47] O. Anunziata, A. Beltramone, M. Martínez, L. López Belon, J. Colloid Interface Sci. 315 (2007) 184–190.
[48] B. Weckhuysen, A. Verberckmoes, A. De Baets, R. Schoonheydt, J. Catal. 166 (1997) 160–171.
[49] B. Weckhuysen, I. Wachs, R. Schoonheydt, Chem. Rev. 96 (1996) 3327–3350.
[50] M. McDaniel, M. Welch, J. Catal. 82 (1983) 98–109.
[51] M. Vuruman, I. Wachs, D. Stufkens, A. Oskam, J. Mol. Catal. 80 (1993) 209–227.
[52] L. Zhang, Y. Zhao, H. Dai, H. He, C.T. Au, Catal. Today 131 (2008) 42–54.
[53] M. Cutrufello, S. De Rossi, I. Ferino, R. Monaci, E. Rombi, V. Solinas, Thermochim. Acta 434 (2005) 62–68.
[54] S. Kumar, N. Hammer, M. Rønning, A. Holmen, D. Chen, J. Walmsley, G. Øye, J. Catal. 261 (2009) 116–128.
[55] S. Wang, K. Murata, T. Hayakawa, S. Hamakawa, K. Suzuki, Catal. Lett. 63 (1999) 59–64.
[56] N. Ikenaga, T. Tsuruda, K. Senma, T. Yamaguchi, Y. Sakurai, T. Suzuki, Ind. Eng. Chem. Res. 39 (2000) 1228–1234.
[57] Y. Ohishi, T. Kawabata, T. Shishido, K. Takaki, Q. Zhang, Y. Wang, K. Takehira, J. Mol. Catal. A: Chem. 230 (2005) 49–58.
[58] Y. Sakurai, T. Suzaki, K. Nakagawa, N. Ikenaga, H. Aota, T. Suzuki, J. Catal. 209 (2002) 16–24.
[59] A. Nijhuis, S. Tinnemans, T. Visser, B. Weckhuysen, Chem. Eng. Sci. 59 (2004) 5487–5492.